EUROPHYSICS LETTERS 10 September 1996

Europhys. Lett., **35** (8), pp. 579-584 (1996)

Complex spatio-temporal dynamics in the near-field of a broad-area semiconductor laser

I. Fischer[1], O. Hess[2], W. Elsäßer[1] and E. Göbel[3]

[1] *Institut für Angewandte Physik*
Schloßgartenstr. 7, TH Darmstadt, D-64289 Darmstadt, Germany
[2] *Institut für Technische Physik, DLR*
Pfaffenwaldring 38-40, D-70569 Stuttgart, Germany
[3] *Physikalisch Technische Bundesanstalt*
Bundesallee 100, D-38116 Braunschweig, Germany

(received 15 May 1996; accepted in final form 12 July 1996)

PACS. 42.65Sg – Dynamics of nonlinear optical systems; optical instabilities, optical chaos, and optical spatio-temporal dynamics.
PACS. 05.45+b – Theory and models of chaotic systems.
PACS. 42.55Px – Semiconductor lasers; laser diodes.

Abstract. – We present the combination of microscopic model calculations and direct experimental evidence for complex spatio-temporal dynamics on a picosecond timescale in the near-field of a broad-area semiconductor laser induced by the interplay of self-focusing, diffraction, and spatial hole burning. We demonstrate the formation of migrating optical filaments within the turn-on dynamics of such a laser and characterize the resulting spatio-temporal complexity via spatio-temporal cross-correlation functions.

The study of optical systems which show the formation of spatio-temporal patterns in the transverse direction is of great current interest [1]-[4]. Among those, the broad-area semiconductor laser plays an important role [5]. Being designed as a semiconductor laser with high output power, the broad-area laser has large technological relevance. However, the increase in output power which is achieved by enlarging the transverse width of the active area to typical sizes of $w = 50\,\mu\text{m}$ to $500\,\mu\text{m}$ results in poor beam quality and coherence properties. This is related to the formation of transverse structures in the near-field of the laser [6]-[8]. Recent model calculations incorporating microscopic-material properties have predicted underlying strikingly complex spatio-temporal dynamics in the light field [9], [10], promoting the broad-area laser as an intriguing model system to study complex spatio-temporal dynamics with one relevant transverse degree of freedom. However, due to the fast time scales of the dynamics, up to now, there has been no direct experimental evidence for such behavior. In this paper we present experimental spatio-temporal images of the near-field of a broad-area laser obtained by single-shot streak camera measurements. For the first time we demonstrate spatio-temporal complexity in the broad-area laser which manifests itself in irregular pulsing and the formation of migrating optical filaments. In direct correspondence with these measurements we present model calculations which microscopically treat the light-matter interaction in the active semiconductor medium along with the macroscopic properties of the laser device structure and thus provide information about the basic mechanisms leading to the observed type of behavior. We study the dynamical behavior of the broad-area laser shortly after turn-on, where we have

access to the build-up process of the spatio-temporal instabilities and, at the same time, avoid junction heating of the laser, thus eliminating the influence of thermal effects on the dynamical behavior.

Our simulations are based on the space-dependent Maxwell-Bloch equations for semiconductor lasers [5] which consist of a system of microscopic-material equations self-consistently coupled to the system of partial differential equations for the counterpropagating complex optical fields $E^+(x,z,t)$ and $E^-(x,z,t)$, the polarizations $P^+(x,z,t)$ and $P^-(x,z,t)$ as well as for the macroscopic charge carrier density $N(x,z,t)$,

$$\pm\frac{\partial}{\partial z}E^{\pm}+\frac{n_{\rm l}}{c}\frac{\partial}{\partial t}E^{\pm} = \frac{i}{2}\frac{1}{k_z}\frac{\partial^2}{\partial x^2}E^{\pm}-\left(\frac{\alpha}{2}+i\eta\right)E^{\pm}+\frac{i}{2}\frac{\Gamma}{n_{\rm l}^2\epsilon_0 L}P^{\pm}, \tag{1}$$

$$\frac{\partial}{\partial t}N = D_{\rm f}\left(\frac{\partial^2}{\partial x^2}+\frac{\partial^2}{\partial z^2}\right)N+\Lambda-\gamma_{\rm nr}N-W+G, \tag{2}$$

with the macroscopic generation rate

$$G=-\chi''\frac{\varepsilon_0}{2\hbar}\left(\mid E^+\mid^2+\mid E^-\mid^2\right)+\left\{\frac{(-i)}{2\hbar}\left[E^+P^{+*}+E^-P^{-*}\right]+\text{c.c.}\right\}. \tag{3}$$

The macroscopic polarization variables are at every spatial point self-consistently linked to the microscopic polarization functions by summation over all momentum states $P^{\pm}=\frac{2}{V}\sum_{\mathbf{k}}d_{cv}(k)\,p^{\pm}_{\mathbf{r}}(k)$, where $d_{cv}(k)$ is the optical dipole matrix element; isotropic Fermi-surfaces are assumed, *i.e.* only $k=|\mathbf{k}|$ is considered. The dynamics of the *microscopic* polarization functions $p^{\pm}_{\mathbf{r}}(k)$ along with those of the distributions of electrons $f^{\rm e}_{\mathbf{r}}(k)$ and holes $f^{\rm h}_{\mathbf{r}}(k)$, where the index $\mathbf{r}=(x,z)$ indicates their parametrical dependence on space, is governed by the microscopic system of material equations presented and discussed in [5], [9]. In the macroscopic wave equations (1), passive wave-guiding properties are represented by $\eta=\eta(x)$ and the confinement factor $\Gamma=\Gamma(x)$ [5]. The (linear) refractive index of the semiconductor material is denoted by $n_{\rm l}$, c is the speed of light, $L=200$ μm the total (longitudinal) length of the laser cavity and ϵ_0 the permittivity of free space. The wave number in the (longitudinal) propagation direction is given by $k_z=n_{\rm l}k_0$, with k_0 being the unperturbed wave number in the vacuum. In (1) and in the generation rate (3), the linear part of the polarization is conveniently included in the linear absorption term α of the semiconductor and in the imaginary part of the susceptibility [10], $\chi''=\alpha n_{\rm l}^2/2\pi\lambda$, respectively, with λ being the laser wavelength. Diffusion of charge carriers is represented in (2) via the diffusion coefficient $D_{\rm f}$, where the influence of spatial variations of N on $D_{\rm f}$ is disregarded. The rates of nonradiative and spontaneous recombination are given by $\gamma_{\rm nr}$ and W, respectively [5]. The transversely dependent injection of charge carriers along the contact stripe is represented by the pumping term $\Lambda(x)=j(x)\eta_i/ed$, where the current density $j(x)$ is uniform along z and transversely only different from zero from $x_0-w/2\le x\le x_0+w/2$, x_0, being the center of the laser stripe, $w=100$ μm its width and $\eta_i=0.8$ the fraction of carriers which actually reaches the active region; e is the charge of an electron and $d=0.15$ μm the (vertical) thickness of the layer. The *longitudinal boundary conditions* are given by $E^+(x,z=0,t)=-\sqrt{R_1}\;E^-(x,z=0,t)$ and $E^-(x,z=L,t)=-\sqrt{R_2}\;E^+(x,z=L,t)$. They represent reflection of the optical fields at the facet mirrors at $z=0$ and $z=L$ of the laser structure. The *transverse boundary conditions* $\partial E^{\pm}/\partial x=-\alpha_w E^{\pm}$ and $\partial N/\partial x=-\tilde{v}_{\rm sr}N$ at $x=+w/2$ as well as $\partial E^{\pm}/\partial x=+\alpha_w E^{\pm}$ and $\partial N/\partial x=+\tilde{v}_{\rm sr}N$ at $x=-w/2$ account for the strong absorption (constant α_w) of the optical fields outside the pumping stripe and surface recombination effects of the charge carriers. The model parameters are adopted from the particular device which we use in our experiments. Before directly comparing our numerical results with corresponding experimental ones, we present a short outline of our experiments. The measurements of the turn-on dynamics

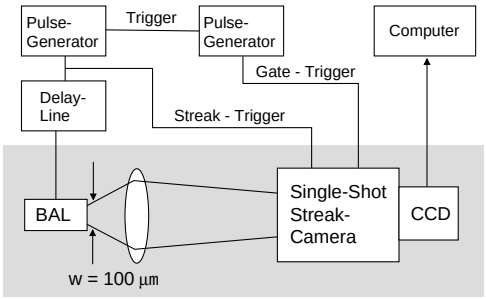

Fig. 1. – Experimental setup for spatio-temporal near-field measurements of a broad-area semiconductor laser.

in the near-field of the broad-area laser have been performed using a GaAs/GaAlAs laser (SDL-2430-C) emitting at $\lambda = 814\,\mathrm{nm}$. Its active region incorporating a quantum well active layer structure has a transverse width $w = 100\,\mu\mathrm{m}$ with an index guiding of the optical field in both the transverse and the vertical direction. The threshold current of the laser is $I_{\mathrm{th}} = 290\,\mathrm{mA}$.

The experimental setup is schematically depicted in fig. 1. A magnified image of the near-field of the light intensity emitted at the output facet is obtained using a microscope objective which projects the output facet of the laser onto the input slit of a Hamamatsu streak camera C1587 with a single sweep unit M1952. This allows to measure single-shot spatio-temporal traces [11] with a time resolution of ~ 50 ps and simultaneous spatial resolution of ~ 3 µm. The main pulse generator serves as current source for the broad-area laser and as trigger source for the streak camera and a second trigger generator. The broad-area laser is driven with rectangular pulses of 25 ns length with a rise time of about 3 ns. The repetition rate of the pulses is 100 Hz, which ensures that junction heating can be avoided. The amplitude of the pulses corresponds to an injection current of ~ 2 times the threshold current. The streak camera is triggered by one single, arbitrarily chosen pulse delayed with respect to the current pulse, allowing to choose the temporal position of the spatio-temporal near-field traces. The traces which are visualized on the phosphor screen of the streak tube are read out by a CCD-camera which is linked to a computer via a frame grabbber card where the traces can be digitally stored.

For these driving conditions the laser emits several transverse modes, while still emitting no more than 3 longitudinal modes corresponding to a spectral width of less than 2 nm which is obtained from time-averaged measurements by an optical spectrum analyzer. The time-averaged near field shows a nearly periodic spatial modulation of the intensity, consisting of different transverse modes, which is a well-known behavior called multi-filamentation, fundamental solitons or higher nonlinear modes [7], [8], [12]-[14]. These operation conditions reflect, as we will demonstrate, complex spatio-temporal behavior. However, for higher currents the behavior can become even more complex [15].

In the following we present and discuss the images of the spatio-temporal intensity distribution, extracted from the numerical modelling $I(x,t)^{\mathrm{num}}$ and directly compare them to those obtained in the measurements $I(x,t)^{\mathrm{exp}}$. In fig. 2 *a*) $I(x,t)^{\mathrm{num}}$ is depicted for the turn-on dynamics of a 100 µm wide broad-area laser. The image shows the temporal evolution of the transversely resolved light intensity emitted from the output facet of the laser. We concentrate on a time window of a length of 1.5 ns taken 8 ns after the first relaxation oscillation. The relaxation oscillations are the dynamical response of the laser on the turn-on current pulse. The selected time window gives a representative image of the spatio-temporal dynamics in the

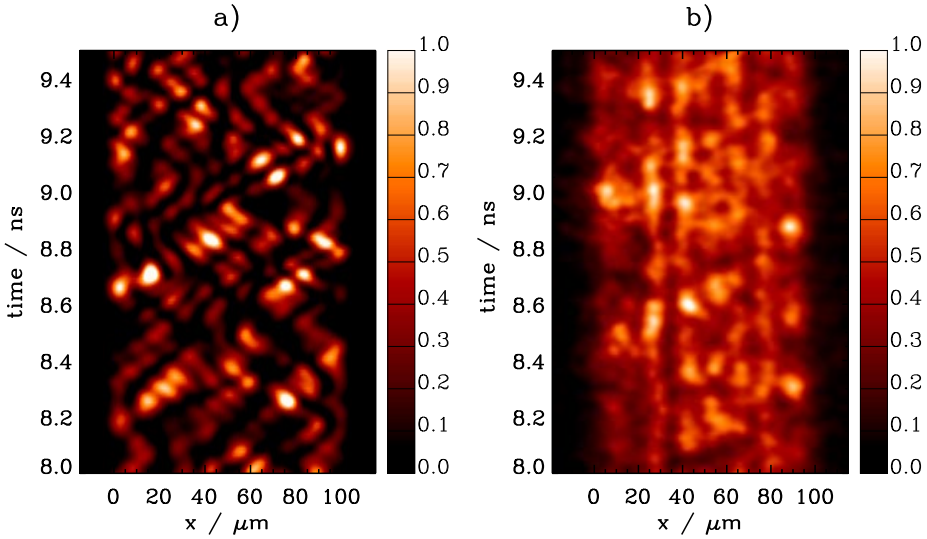

Fig. 2. – Spatio-temporal near-field images of the emitted light intensity: *a*) $I(x,t)^{\mathrm{num}}$ from numerical modelling, *b*) $I(x,t)^{\mathrm{exp}}$ from measurements.

post-relaxation oscillation period [9]. Light red shading in the color images corresponds to high values of $I(x,t)$ and dark colors to low intensities. In the complex spatio-temporal dynamics we observe bewilderingly irregular pulsing behavior and migrating filament-like structures. The numerical results shown in fig. 2 *a*) reveal that it takes about $\Delta t \simeq 500$ ps for an optical filament to migrate from one edge of the laser to the opposite one. The spatial width of such a filament is $s \simeq 10$ to 20 μm. In fig. 2 *b*) we have depicted a typical experimental trace $I(x,t)^{\mathrm{exp}}$ obtained by the single-shot streak camera (cf. fig. 1) corresponding to the situation in fig. 2 *a*). In our experiments, the migrating filaments can indeed be clearly recognized next to the superimposed nearly static modulation of the near-field intensity. This is the first direct proof for the predictions of the numerical modelling. Clearly, this is of substantial interest for the study of spatio-temporal structure formation in general. In our experiments the width of the migrating filaments is $s \simeq 10$ to 20 μm; it takes them about $\Delta t = 200$ to 500 ps to migrate from one edge of the active region to the other one. While the static modulation depends on the pumping and on the waveguiding properties [7], [8], [12], [16], we obtain via analysis of the migrating filaments additional information on the spatio-temporal instabilities with the coupling strength of neighboring transverse positions. The experimentally determined migrating filamentary behavior is in reasonable agreement with the results from our numerical modelling. The question that arises is: *what is the reason for this dynamic filamentation?* From the modelling we can identify the interplay of self-focussing, diffraction and spatial hole burning which again depends on spatial carrier diffusion as the relevant physical mechanisms. In a simple picture this can be understood as follows. The self-focussing tends to guide high intensities in a self-created waveguide. The gain medium shows spatial hole burning in the regions of high intensity resulting in a decrease of the optical gain. Thus, in the neighboring regions the gain is higher. In addition, diffraction couples light into this neighboring region so that the spot of high intensity starts to migrate. At the edges of the active area coupling via diffraction occurs only to one side, leading to the change of direction of migration.

To quantify the spatio-temporal dynamical behavior of both simulated and measured near-

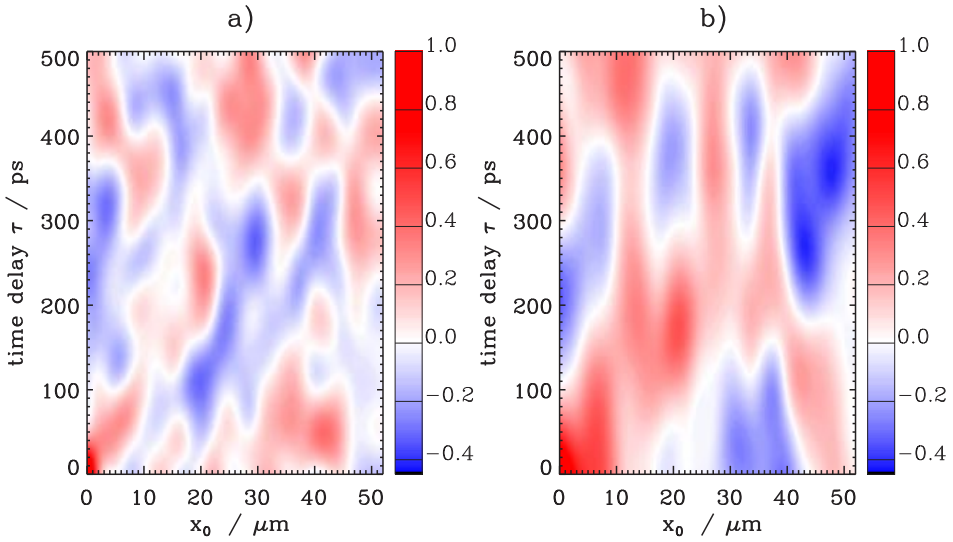

Fig. 3. – Spatio-temporal cross-correlation functions calculated from the near-field traces of the emitted light intensity: *a*) $g(x_0,\tau)^{\mathrm{num}}$ from numerical modelling, *b*) $g(x_0,\tau)^{\mathrm{exp}}$ from measured traces.

field traces, we calculate the spatio-temporal cross-correlation function [9]

$$g(x_0,\tau) = \frac{\langle \delta I(x_c - x_0, t)\ \delta I(x_c + x_0, t+\tau)\rangle_t}{\sqrt{\langle \delta I^2(x_c - x_0, t)\rangle_t}\ \sqrt{\langle \delta I^2(x_c + x_0, t)\rangle_t}}, \tag{4}$$

where x_c is the center of the laser. $\langle \ldots \rangle_t$ denotes the average over time t,$I(x,t)$ is the field intensity at the laser facet at the transverse position x and $\delta I(x,t) = I(x,t) - \langle I(x,t)\rangle_t$ is the deviation of the intensity at the point x from its temporal average $\langle I(x,t)\rangle_t$. The correlation function $g(x_0,\tau)$ provides information about the averaged dynamical correlation of two points which are chosen to be located symmetrically at a distance x_0 from the center of the active region and which have a time delay τ with respect to each other. Note that the correlation function $g(x_0,\tau)$ quantifies not only the distinct spatial or temporal correlation properties but, in addition, the coupled spatio-temporal correlations. In fig. 3 images of $g(x_0,\tau)^{\mathrm{num}}$ and $g(x_0,\tau)^{\mathrm{exp}}$ for the near-field traces of fig. 3 are depicted, where dark red represents high correlation, dark blue strong anti-correlation and white no correlation. They illustrate and quantify the enhanced *spatio-temporal correlation* induced by the migrating filaments which manifests itself in correlations running diagonally, *i.e.* from down left to up right, in the (x_0,τ)-plane. We find that the main features characterizing the spatio-temporal behavior of the laser can be recognized in both correlation functions, although the complexity in the simulated spatio-temporal images appears to be somewhat higher in the simulation than in the experiments. In fig. 3 *a*), where $g(x_0,\tau)^{\mathrm{num}}$ is depicted, one can clearly recognize the fast decay of correlation with respect to both space and time. The correlation resulting from the migrating filaments can be recognized in the diagonally enhanced correlation from $(x_0,\tau) = (0,0)$ to $(50\ \mu\mathrm{m}, 500\ \mathrm{ps})$. Furthermore, note the spot of high correlation for $(x_0,\tau) = (45\ \mu\mathrm{m}, 50\ \mathrm{ps})$ which reflects the existence and correlation of more than just one migrating filament: if one filament reaches the edge of the active region, it is probable for another one to be at the opposite edge. By this means, the optical filaments effectively use the dynamic variations in the inversion: a filament migrates in between two pulses of a prevailing filament. The spatio-temporal correlation $g(x_0,\tau)^{\mathrm{exp}}$ drawn from the experimental spatio-temporal image is

depicted in fig. 3*b*). It clearly shows the fast decay with respect to space and time and the diagonally enhanced correlation. Due to the larger variation of their transit time the correlation pertaining to the migrating filaments is somewhat broader in $g(x_0,\tau)^{\mathrm{exp}}$ than in $g(x_0,\tau)^{\mathrm{num}}$. The influence of counter-migrating filaments, which is represented by the enhanced correlation at large spatial distances and short delay times, is less striking in $g(x_0,\tau)^{\mathrm{exp}}$, but also present in the region of $(x_0,\tau) = (45\ \mu\mathrm{m}, 100\ \mathrm{ps})$. Indeed, this can already be deduced from the original experimental spatio-temporal trace itself showing additional migrating filaments which are weaker than in the simulations. However, the main aspects of spatio-temporal complexity, drawn from direct comparison of experiment and modelling as well as from the spatio-temporal correlation functions, show close correspondence. In particular, the velocity of migration and width of the migrating optical filaments are even in quantitative agreement.

In conclusion, we have presented the first cohesive investigation of the spatio-temporal near-field dynamics of a broad-area semiconductor laser involving experiments and numerical modelling. We show that the fundamental interaction between light and the active semiconductor medium, *i.e.* the balance between diffraction and self-focusing effects as well as carrier diffusion, leads to the formation of complex spatio-temporal structures. Our results are not only relevant for the understanding of this technologically important laser device but, in particular, are a paradigm for spatio-temporal pattern formation in active systems with one relevant transverse degree of freedom.

***

We would like to thank U. Denzer from Hamamatsu Photonics Germany GmbH for his support and for providing the single-shot unit for our measurements, M. Preis for technical support and the Deutsche Forschungsgemeinschaft for the funding within the Sonderforschungsbereich 185.

REFERENCES

[1] Lugiato L. A., Prati F., Narducci L. M., Ru P., Tredicce J. R. and Bandy D. K., *Phys. Rev. A*, **53** (1988) 3847.
[2] Abraham N. B. and Firth W., *J. Opt. Soc. Am. B.*, **7** (1990) 951.
[3] Lugiato L. A., *Chaos, Solitons Fractals*, **4** (1994) 1251.
[4] Harrison R. G. and Uppal J. S. (Editors), *Nonlinear Dynamics and Spatial Complexity in Optical Systems, SUSSP Proceedings*, Vol. **41** (Institute of Physics publishing, Bristol and Philadelphia) 1992.
[5] Hess O. and Kuhn T., *Prog. Quantum Electron.*, **20** (1996) 85.
[6] Larsson A., Salzman J., Mittelstein M. and Yariv A., *J. Appl. Phys.*, **60** (1986) 66.
[7] Chang-Hasnain C. J., Kapon E. and Colas E., *IEEE J. Quantum Electron.*, **QE-26** (1990) 1713.
[8] Lang R. J., Larsson A. G. and Cody J. G., *IEEE J. Quantum Electron.*, **QE-27** (1991) 312.
[9] Hess O., *Chaos, Solitons Fractals*, **4** (1994) 1597.
[10] Hess O., Koch S. W. and Moloney J. V., *IEEE J. Quantum Electron.*, **QE-31** (1995) 35.
[11] DeFreez R. K., Bossert D. J., Yu N., Hartnett K. and Elliott R. A., *Appl. Phys. Lett.*, **53** (1988) 2380.
[12] Mehuys D., Lang R. J., Mittelstein M., Salzman J. and Yariv A., *IEEE J. Quantum Electron.*, **QE-23** (1987) 1909.
[13] Mc Laughlin D. W., Moloney J. V. and Newell A. C., *Phys. Rev. Lett.*, **51** (1983) 75.
[14] Khitrova G., Gibbs H. M., Kawamura Y., Iwamura H. and Ikegami T., *Phys. Rev. Lett.*, **70** (1993) 920.
[15] Fischer I., Hess O. and Elsäßer W., unpublished.
[16] Paxton A. H. and Dente G. C., *J. Appl. Phys.*, **70** (1991) 2921.